Collective Mechanism for the Evolution and Self-Termination of Vertically Aligned Carbon Nanotube Growth

Mostafa Bedewy,[†] Eric R. Meshot,[†] Haicheng Guo,[†] Eric A. Verploegen,[‡] Wei Lu,[†] and A. John Hart*[,†]

Department of Mechanical Engineering, University of Michigan, 2350 Hayward Street, Ann Arbor, Michigan 48109, and Department of Materials Science and Engineering, Massachusetts Institute of Technology, 77 Massachusetts Avenue, Cambridge, Massachusetts 02139

Received: May 4, 2009; Revised Manuscript Received: October 12, 2009

We explain the evolution and termination of vertically aligned carbon nanotube (CNT) "forests" by a collective mechanism, which is verified by temporal measurements of forest mass and height, as well as quantitative spatial mapping of CNT alignment by synchrotron X-ray scattering. We propose that forest growth consists of four stages: (I) self-organization; (II) steady growth with a constant CNT number density; (III) decay with a decreasing number density; and (IV) abrupt self-termination, which is coincident with a loss of alignment at the base of the forest. The abrupt loss of CNT alignment has been observed experimentally in many systems, yet termination of forest growth has previously been explained using models for individual CNTs, which do not consider the evolution of the CNT population. We propose that abrupt termination of CNT forest growth is caused by loss of the self-supporting structure, which is essential for formation of a CNT forest in the first place, and that this event is triggered by accumulating growth termination of individual CNTs. A finite element model accurately predicts the critical CNT number density at which forest growth terminates and demonstrates the essential role of mechanical contact in maintaining growth of self-assembled films of filamentary nanostructures.

Despite recent advances in our understanding of the multivariate nature of carbon nanotube (CNT) growth by chemical vapor deposition (CVD), the mechanism of growth termination is still not fully understood. This limits the efficiency of CNT manufacturing, restricts commercial viability of applications[1] that require bulk quantities of CNTs, and prevents us from realizing indefinitely long strands of continuous CNTs as next-generation structural fibers and electrical transmission lines. Significant study has focused on understanding the mechanisms that limit the growth of individual CNTs, and it has been suggested that growth termination can be caused by evaporation, contamination, alloying, or overcoating of the catalyst particle that resides at the base or tip of the growing CNT.[2−4] Interestingly, the longest known CNTs have been grown as "floating" isolated CNTs in the CVD atmosphere,[5] suggesting coupling inherently present among CNTs within a forest are a limiting condition for achieving indefinite CNT growth. However, considering that at least tens of thousands of CNTs must be packed to create even a micrometer diameter fiber, self-assembly of CNTs during growth is likely necessary for efficient manufacturing of large-scale aligned CNT materials.

Vertically aligned CNT "forests" typically comprise billions of CNTs per square centimeter on a substrate and are a model system for understanding the collective mechanics of CNT growth. Further, owing to their anisotropic structure and the outstanding properties[6] of individual CNTs, CNT forests are widely attractive for use as mechanical, electrical, and thermal interface layers,[7−9] electrochemical storage devices,[10] and membranes for gas, liquid, and biological separations.[11−14] For these and other applications, it is critical to manufacture CNT forests having spatially uniform characteristics.

A CNT forest forms when CNTs self-orient due to crowding during the initial stage of growth, and along with appropriate control of the CVD conditions, CNT forests can reach heights of several millimeters or more. Recent studies have shown the importance of oxygen,[15] hydrogen,[15] water vapor,[16] and carbon dioxide[17,18] in mediating gas-phase reactions in the CVD atmosphere, controlling deposition of carbon at the nanoparticle growth sites, and prolonging the duration of catalyst activity. Small amounts of these species, in addition to fluctuations in ambient pressure,[4] have been shown to affect consistency and repeatability of experimentation. CNT forest growth was also prolonged by adjusting the stoichiometry of bimetallic catalyst particles[19] and by stabilizing the underlying Al_2O_3 support by doping with a rare earth element such as lanthanum (La).[20] The latter approach was used to grow CNT forests as high as 18 mm.[21] However, in spite of all these efforts, termination of CNT forest growth has not been overcome.

Further, previous attempts to understand the limiting mechanisms of CNT forest growth have represented the growth kinetics by the evolution of the forest height with time. These studies have assumed that the areal density of CNTs remains constant throughout the forest and have explained forest termination using behavior expected for an *individual* CNT−catalyst system. However, considering that a forest is a *population* of CNTs having a certain diameter distribution and that interactions among CNTs create and maintain the aligned morphology, it is necessary to adopt a holistic approach that accounts for the collective behavior of CNTs.

* To whom correspondence should be addressed. E-mail: ajohnh@umich.edu. Phone: 734-615-6146.
[†] University of Michigan.
[‡] Massachusetts Institute of Technology.

10.1021/jp904152v CCC: $40.75
Published on Web 10/29/2009

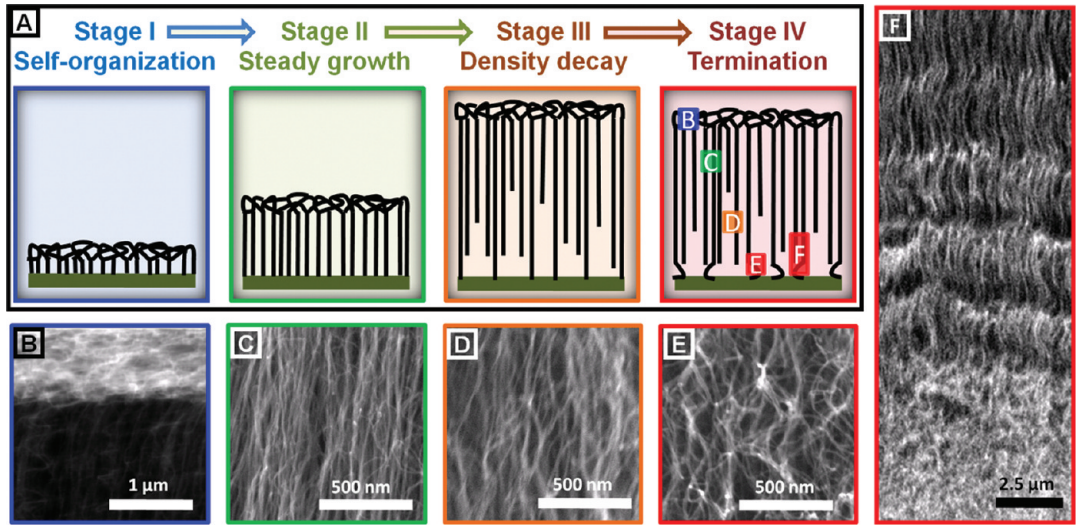

Figure 1. Collective growth mechanism of a CNT forest: (A) growth stages and SEM images of (B) tangled crust at the top of forest, (C) aligned and dense morphology near the top of a self-terminated forest, (D) less aligned and less dense morphology in the lower region of a self-terminated forest, and (E, F) randomly oriented morphology at the bottom, induced by the loss of the self-supporting forest structure.

In this study, we explain the evolution and termination of CNT forest growth based on a collective model consisting of four stages, as illustrated in Figure 1A:

I. Nucleation and self-assembly of randomly oriented CNTs into a vertically aligned forest structure.
II. Steady growth, wherein the number density of growing CNTs remains constant with time.
III. Density decay, wherein the number density of CNTs within the forest decreases with time.
IV. Abrupt self-termination, wherein forest growth ceases suddenly, and is accompanied by a loss of CNT alignment at the interface between the CNTs and the substrate.

This model is verified by combining *in situ* measurements of forest height during growth, spatial mapping of CNT alignment by synchrotron X-ray scattering, and *ex situ* measurements of CNT forest mass versus height and growth time. Further, a finite element model considering the effect of CNT−CNT spacing and contact on the mechanical stiffness of a CNT forest accurately predicts the CNT areal density at which termination is observed experimentally.

Therefore, we suggest that abrupt termination of CNT forest growth is caused by loss of the self-supporting structure that is essential for organization of a CNT forest in the first place. The proposed mechanism supports several previously unexplained observations of abrupt growth termination using both *in situ* and *ex situ* height measurements of single-wall (SWNT) and multiwall CNT (MWNT) forests.[4,22−27] Further, filamentary nanostructures are replete in man-made and natural systems, and this study further reveals how interactions among such structures not only govern their collective behavior but are also critical to their self-organization and morphological evolution.

CNT growth was performed using both a horizontal quartz tube furnace (Thermo-Fisher Mini-Mite, 22 mm inner diameter, 12 in. heated length), and a "cold wall" reactor system (Absolute Nano SabreTube) wherein the growth substrate rests on a resistively heated silicon platform.[28,29] In all experiments, the growth substrate was 1/10 nm Fe/Al_2O_3, deposited on thermally oxidized (100) silicon wafers by electron beam evaporation. After installing the substrate and purging the reactor, the catalyst was heated to the growth temperature in flowing H_2/He, and then C_2H_4 was added for the growth duration (t), which ranged from 2.5 to 30 min. The growth process parameters are further detailed in the Supporting Information. Feedback control of temperature and flow was automated using LabVIEW (National Instruments). With the heated-platform reactor, forest height was measured in real time during growth using a noncontact laser displacement sensor (Keyence LK-G152). This sensor was also used for *ex situ* forest height measurements. Forest mass was measured using an electronic scale (Ohaus Discovery DV215CD) with accuracy 0.01 mg, by weighing the silicon substrate after CNT growth, before and after delaminating the CNT forest. SEM imaging was performed using a Philips XL30-FEG. X-ray scattering was performed at the G1 beamline at the Cornell High Energy Synchrotron Source (CHESS), with a slit-collimated beamspot size of ≈100 μm.

SEM images (Figure 1B) show the morphological evolution of a CNT forest during growth, starting (stage I) with formation of a thin "crust"[30] of randomly oriented CNTs that resides on the top of the forest after alignment emerges. The forest sidewall then exhibits a uniform, aligned, and dense texture (Figure 1C) that extends downward below the crust and into the density decay region (Figure 1D). It is important to note that SEM images are not used to infer information about the CNT number density, as the CNTs are likely bundled together, and the focal depth of SEM makes it difficult to precisely discern density differences unless more involved techniques (e.g., stereo imaging[31]) are used. Nevertheless, SEM confirms the evolution of CNT alignment and morphology. Finally, the base of a CNT forest, which has been grown until self-termination occurs (stage IV), transforms to a distinctly rippled and tangled morphology (Figure 1E, F). This morphology is typically restricted to within several micrometers from the substrate and has been observed in several previous studies but has not yet been explained.[4,27] It is important to note that this bottom layer may appear to have a high packing density of unoriented CNTs even though the number density of CNTs (i.e., the number of continuous CNTs that are growing from the substrate) is low. This is presumably because the CNTs continue to grow and crowd one another for a short duration after the forest loses its self-supporting structure. Nevertheless, owing to the small thickness of this layer as compared to the forest height, its contribution in the total forest mass is believed to be negligible.

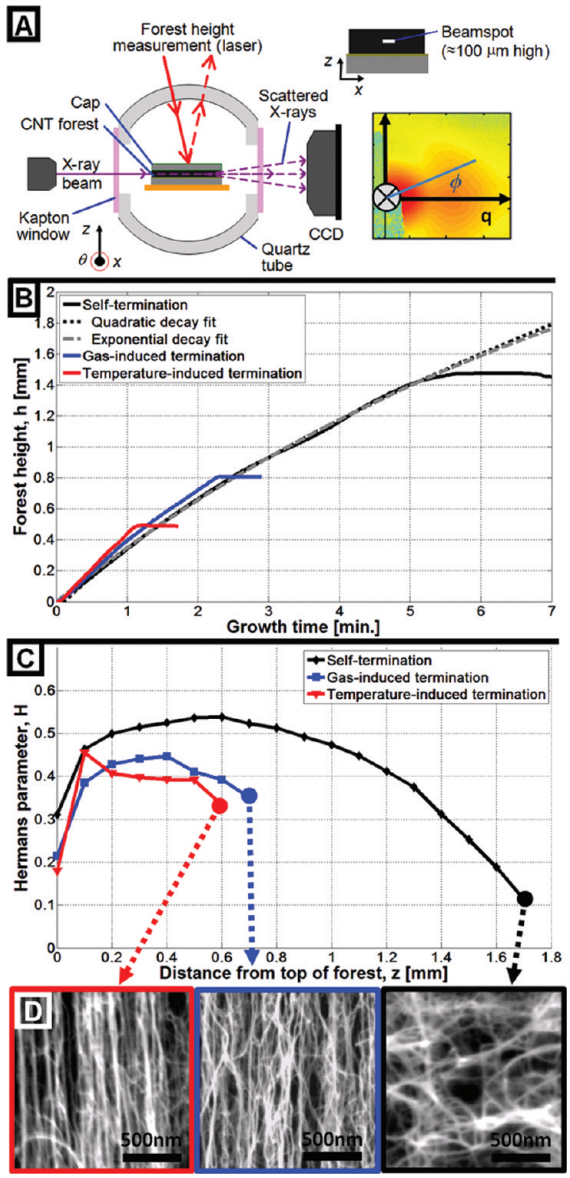

Figure 2. Measurements of forest height and CNT alignment using a "cold wall" reactor, comparing self-terminated forest growth with control experiments where termination was induced by cooling the substrate and discontinuing the carbon supply: (A) cross-section setup of reactor mounted in synchrotron beamline; (B) *in situ* forest height measurements; (C) mapping of Hermans orientation parameter; (D) SEM images of forest base morphology. Data in (C) were taken by scanning the forests mounted in the reactor immediately after growth.

The abrupt termination of CNT forest growth is further demonstrated by quantifying the evolution of CNT forest height and alignment during growth. Figure 2A shows a schematic representation of our unique reactor configuration which enables *in situ* measurement of CNT forest height during growth, and acquisition of small-angle X-ray scattering (SAXS) patterns by positioning the synchrotron beam (by moving the reactor on a motorized stage) to pass through at a desired section of the forest. Scattering data were obtained during growth, by positioning the X-ray beam just above the interface between the CNT forest and the substrate; and after growth, by scanning the forest from bottom to top. The CNT alignment within a forest is quantified by calculating the Hermans orientation parameter (H)[32]

$$H = \frac{1}{2}(3\langle\cos^2\phi\rangle - 1) \quad (1)$$

$$\langle\cos^2\phi\rangle = \frac{\int_0^{\pi/2}(I(\phi)\sin\phi\cos^2\phi)\,d\phi}{\int_0^{\pi/2}(I(\phi)\sin\phi)\,d\phi} \quad (2)$$

Here, ϕ is the azimuthal angle, shown in the inset of Figure 2A. $I(\phi)$ is the corresponding scattered intensity, measured at the radial location corresponding to the local maximum of intensity arising from form factor scattering of the CNTs.[33] The morphological evolution was corroborated by scattering data taken both during and after growth, and data discussed below was taken by scanning the forests mounted in the reactor immediately after growth.

Figure 2B shows *in situ* measurements of the height evolution of a forest that self-terminates and of forests which are terminated prematurely by rapidly cooling the substrate or stopping the flow of C_2H_4/H_2 while maintaining the substrate temperature. As seen in Figure 2C, H increases sharply at the top of a forest, representing the transition from tangled to vertically aligned morphology during the first stage of growth. H then remains approximately constant as growth proceeds, and then it decays steeply toward zero before growth terminates, indicating the onset of disordered CNTs. In agreement with the morphological evolution indicated by the calculated H values, SEM images (Figure 2D) show that the self-terminated forest exhibits disorder at its base, yet the intentionally terminated forests exhibit strong alignment at the base. This demonstrates that the loss of alignment is a signature of growth self-termination, and is not caused by cooling the reactor or by an abrupt decrease in the carbon concentration in the CVD atmosphere, as demonstrated in Figure 2B. The ≈100 μm height of the X-ray beamspot limits the spatial resolution of H; therefore, the apparent thickness of the tangled crust is much larger than observed by SEM imaging, and the rate of decline in alignment during the decay and termination stages is more rapid than determined by SAXS mapping.

While measurements of the CNT forest height versus time have previously been used as a direct estimate of the reaction rate,[34−36] measuring the time evolution of CNT forest mass provides a needed complement to the forest height data in revealing the true growth kinetics. Figure 3A shows how both the forest height and the mass per unit area change with time. Each point on this plot is an average of three forests (5 × 5 mm^2 area), all grown in the same position along the length of the tube furnace, and measured after growth. As was also observed *in situ*, the forest height increases in an essentially linear fashion with time until abrupt termination occurs; however, the rate of mass increase begins to decrease long before the forest height stops increasing. Significant amorphous carbon accumulates[37] on the CNT sidewalls when the sample is left in the furnace for a long duration after growth termination; however, before termination, amorphous carbon accumulation is an insignificant fraction of the measured mass and therefore does not affect the kinetics. This is shown by thermogravimetric analysis (TGA) of CNT forests grown in the same hot-walled reactor, which we have reported in another publication.[38]

The faster rate of height increase, as compared to mass increase during the later stage of growth, indicates that the number density of CNTs growing at the substrate begins to decrease long before termination occurs. The time evolution of the CNT number density during growth is shown in Figure 3B

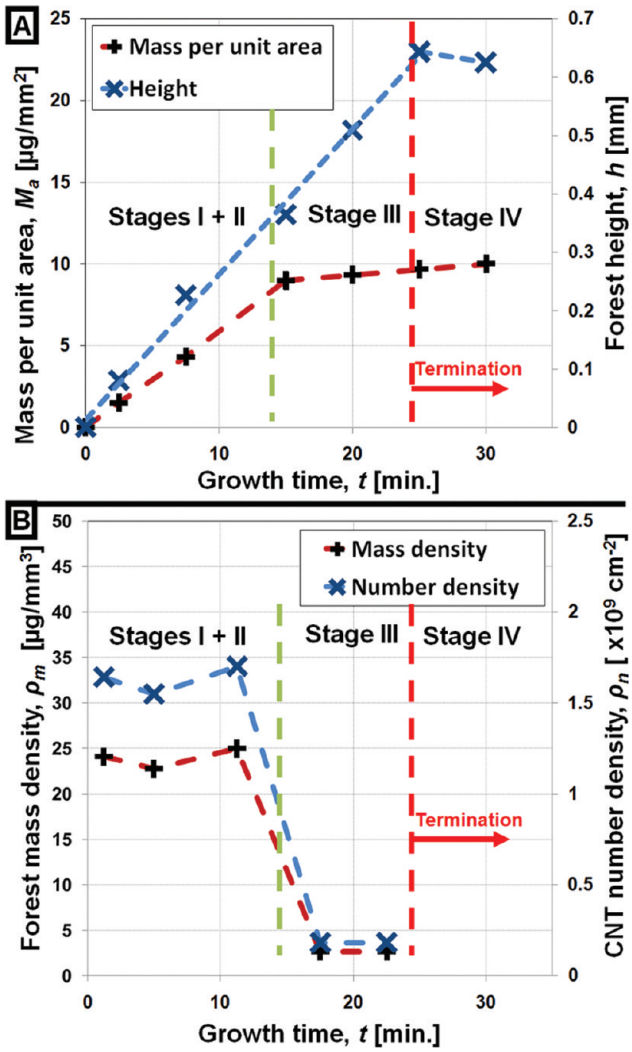

Figure 3. *Ex situ* measurements of the time evolution (A) forest mass and height, and (B) differential mass density and CNT number density, for samples grown in a conventional "hot wall" tube furnace.

and is estimated by first calculating the differential change in the mass density between forests grown for slightly different durations. From this differential mass density, the CNT number density is calculated as

$$\rho_m = \frac{M_a(t_n) - M_a(t_{n-1})}{h(t_n) - h(t_{n-1})} \tag{3}$$

$$\rho_n = \frac{\rho_m/\rho}{\frac{\pi}{4}(d_o^2 - d_i^2)} \tag{4}$$

For this calculation, we consider the CNTs to be continuous straight hollow cylinders of graphite ($\rho = 2.2$ g/cm^3), having outer diameter $d_o = 11$ nm, and inner diameter $d_i = 6$ nm. The diameters are measured by fitting the SAXS patterns with a form factor model for a lognormally distributed population of hollow cylinders, and this method agrees closely with TEM diameter measurements in our previous work.[33,38] A ratio of 0.6 between the inner and outer diameter of the CNTs appropriately fits the scattering data and agrees with TEM analysis. Using SAXS to map the CNT diameter versus vertical position in these forests suggests that the CNT diameter may change only by 5−10%

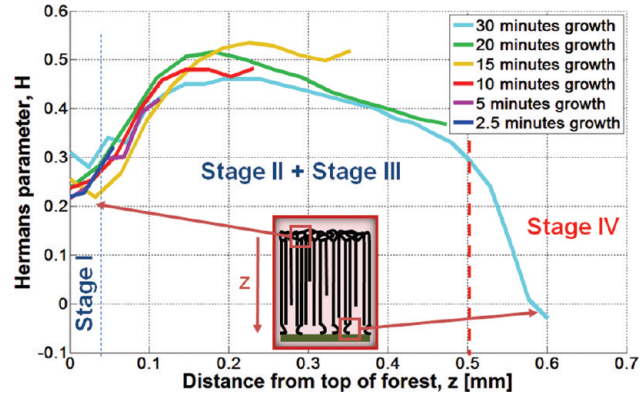

Figure 4. Time evolution of Hermans orientation parameter for forests grown for different durations in a "hot wall" tube furnace.

during growth (Figure S3). Therefore, our assumption of constant CNT diameter along the forest height does not significantly affect the number density calculations. Clearly, it is not fully accurate to assume that the CNTs are straight, and this assumption becomes less accurate as the CNT alignment within the forest degrades. The assumption of straight CNTs therefore underestimates the magnitude and rate of the number density decay, as the true length of a CNT will be greater if it is not fully perpendicular to the substrate.[39]

The analysis of the time evolution of forest density allows us to elucidate the proposed stages of the collective growth mechanism, as indicated in Figure 3. Steady growth (stage II) occurs when the differential mass density remains essentially constant (≈24 μg/mm^3) with growth time, and this lasts for ≈15 min. Then, the density decays (stage III) sharply by nearly an order of magnitude (≈3 μg/mm^3). Termination (stage IV) occurs 10−15 min later ($t = 25$ min), when the forest height abruptly stops increasing. CNT forests grown for different durations in a tube furnace were also mapped by SAXS after growth, and the resulting trends of Hermans orientation parameter are shown in Figure 4. This corroborates the emergence, stabilization, and decay of CNT alignment that is also observed in Figure 2C, suggesting that the collective growth mechanism applies to both "hot wall" and "cold wall" CVD systems. Further, even considering that the X-ray beam height is ≈100 μm compared to the maximum forest height of ≈600 μm, it is apparent that the CNT alignment decays gradually before suddenly transitioning to a random morphology when growth self-terminates.

Raman spectroscopy, shown in Figure S4, was used to compare the quality of CNT forests grown for different times. The slight variation in the G/D ratio obtained from sample to sample suggests that the quality of CNTs does not deteriorate significantly throughout the growth process. Nevertheless, a slight decrease in G/D ratio was observed within each sample when scanning from top to bottom. This may be caused by the accumulation of defects in CNTs prior to their individual growth termination or may be an effect of the increasing tortuosity of CNTs as the number density decays. Further understanding of this behavior is beyond the scope of this paper, and this is a subject of ongoing study.

Our experiments demonstrate that the decay of the number density of growing CNTs within the forest eventually renders the forest incapable of sustaining a self-supporting morphology, and that abrupt termination of growth occurs when the CNT number density at the base of the forest drops below a critical value. This behavior is captured analytically using a finite element model (ABAQUS), which enables us to study the dependence of self-supporting CNT−CNT interactions on the

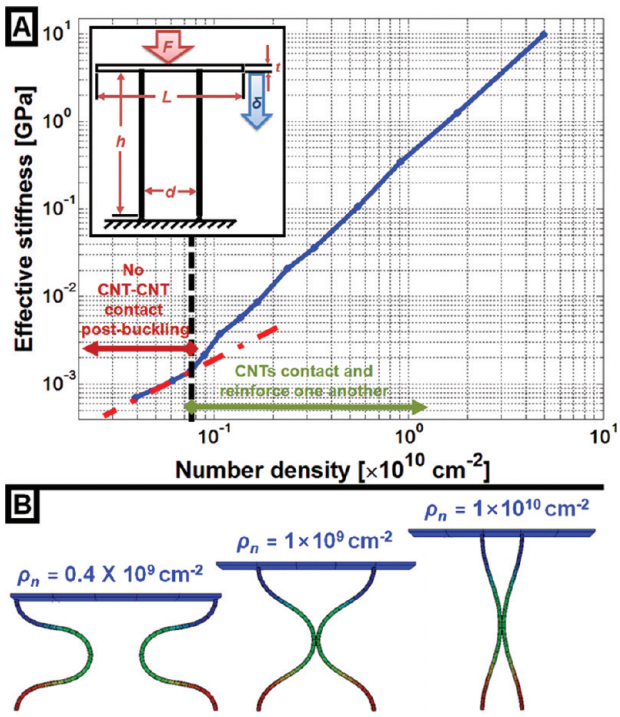

Figure 5. Finite element modeling of CNT buckling and pairwise reinforcement: (A) dependence of the effective modulus on the areal density of CNTs, with inset showing the model for a pair of CNTs; (B) representative deformed configurations of pairs of CNTs.

spacing between CNTs within the forest. We consider a simplified two-dimensional case where a pair of CNTs that lie in the same plane (Figure 5A), are modeled as hollow cylinders ($d_i = 6$ nm, $d_o = 10$ nm, $E = 1$ TPa, $\nu = 0.3$) fixed to a rigid top panel and pinned to a bottom substrate. We believe this simplification is justified by the presence of the attractive van der Waal's potential between CNTs, which is expected to draw CNTs together when they are in proximity. To simulate the deformation of this two-CNT system, we first perform an eigenvalue analysis to determine the shape of the first buckling mode of an individual CNT and then impose the buckled shape as the starting condition for each CNT in the two-CNT system. Then, the two-CNT system is deformed by applying a downward pressure to the top panel, which is restricted to move only in the vertical direction. The initial buckled shape guarantees that the two CNTs will deform toward each other and is representative of the actual case where CNTs are inherently tortuous and thus will not behave as perfect columns.

An effective modulus of the two-CNT system is defined as $K = \sigma/\varepsilon$, where $\sigma = F/2d^2$ is the force per unit area (pressure) acting on the top panel, where d is the inter-CNT spacing, and $\varepsilon = \delta/h$ is the ratio of displacement (δ) divided by the initial length (h) of the CNTs. By changing the distance between the pair of CNTs in this simple postbuckling mechanical model, we study how the effective modulus of a CNT forest depends on the number of CNTs per unit area (areal density), as shown in Figure 5B. In a sparse arrangement, CNTs do not contact each other, and consequently, stiffness increases linearly with number density. This linear increase proceeds until a critical value of $\approx 8 \times 10^8$ CNTs/cm^2, at which point the CNTs contact after deformation, resulting in a nonlinear increase in K with increasing number density. This critical value, noted by a vertical line in Figure 5B, is believed to correspond to the threshold CNT number density needed to maintain a self-supporting structure. This is close to the value of $\approx 1.7 \times 10^9$ CNTs/cm^2 measured in our experiments at the transition between density decay (stage III) and termination (stage IV) and may also represent the threshold density[40] needed to form the self-supporting forest structure at the start of the growth process. As the number density increases beyond the threshold, the consequent deformation needed to establish contact between neighboring CNTs decreases. Therefore, the alignment of a CNT forest decreases gradually as the number decays before reaching the threshold for self-termination. Although this model simplifies the true structure of a CNT forest, which contains isolated CNTs and bundles, the qualitative insights complement the experimental observations that CNT forest number density and alignment are coupled and that CNT−CNT contact creates essential mechanical reinforcement. Further details and results from the model are in the Supporting Information.

Previous investigations of the time evolution of CNT forest height have concluded that, depending on the reaction conditions, the growth rate may be limited by the reaction rate at the catalyst or by diffusion of the carbon precursor to the catalyst.[34] In the former case, the forest height is linear with time,[35] and in the latter case, quadratic decay ($h \propto t^{1/2}$) is observed.[36] Our investigation shows that these kinetic models may be appropriate for the steady growth stage, as indicated by the fits to our real time height data (Figure 2B); however, these models predict that forest growth will proceed beyond the abrupt halt that is observed in the real time data and therefore do not address the termination mechanism. Further, the rate of mass accumulation is a more direct measure of the reaction rate and therefore is a necessary complement to the CNT forest height in understanding the growth kinetics. Because the rate of mass increase begins to decay while the rate of height increase remains constant, it is evident that some CNTs stop growing *individually* before the forest height stops increasing. Meanwhile, the forest height rises in an undisturbed fashion as a result of the growth of the remaining population that has not terminated yet.

Recent attention has focused on the use of oxygen-containing carbon precursors and additives to increase the catalyst activity and possibly extend the lifetime of CNT forest growth. It has been demonstrated that presence of water vapor in the growth atmosphere can slow Ostwald ripening of Fe by hydroxylation of the alumina support.[41] Studies of water-assisted[16,42] CVD proposed that the rate of forest height increase decays exponentially due to gradual catalyst poisoning,[43] or that forest growth stops abruptly when the catalyst is overcoated with amorphous carbon,[4] even though a small ($\approx$100 ppm) water concentration in the CVD ambient can enhance the catalyst lifetime by etching amorphous carbon from the catalyst surface.[44,45] Further, past studies considered the behavior of an *individual* CNT as representing the kinetic behavior of the forest. It was also shown that the mass of a forest grown by water-assisted CVD evolved linearly with growth time,[46] yet this study only addressed the steady growth stage. We have found that adding a small concentration of ethanol to our C_2H_4/H_2/He atmosphere prolongs the catalyst lifetime to over 60 min;[47] however, SAXS mapping demonstrates that the alignment decays in a similar fashion to the forests grown without added ethanol. Therefore, we believe the density decay mechanism governs collective termination even in the presence of oxygen-containing additives.

We hypothesize that growth termination of an individual CNT is governed by the lifetime of the catalyst particle, which depends on its diameter, surface conditions, and other factors. Chemical analysis performed on catalyst substrates after manual delamination of CNT forests indicates that Fe diffuses through

the supporting Al_2O_3 layer and into the underlying SiO_2, and thus diffusion of Fe could be responsible for the observed density decay. This behavior may be affected by engineering the morphology (e.g., porosity) and thickness of the supporting Al_2O_3 layer.[48,49] However, our ongoing work also demonstrates that the forest growth rate and catalyst lifetime (i.e., the duration before self-termination occurs) strongly depend on the hydrocarbon composition of the reactant atmosphere. Therefore, multiple factors may contribute to collective termination, and one factor may dominate under particular conditions. The same is likely true for the rate of decay in the number density of growing CNTs, which may differ considerably on the basis of the growth conditions (i.e., catalyst, carbon source, temperature). As an opposite limiting case, simultaneous growth termination of all CNTs would presumably cause termination of forest growth without a loss of alignment at the base. Thus, further study is needed to assess the generality of the proposed mechanism; however, we note the coincidence of abrupt termination with a loss of CNT alignment has been observed in many recent studies using widely different CNT forest growth recipes.[4,22−27]

Further, it was recently suggested that deactivation of an individual CNT causes buildup of mechanical stress in the forest due to coupling among the tubes at the tangled top layer and that the resulting force at the forest base eventually exceeds the driving chemical potential for the growth reaction, halting forest growth.[50] While this mechanochemical termination mechanism may be possible, in our experiments the decay of the CNT population is gradual and that the role of CNT−CNT interactions in maintaining a self-supporting structure is essential for continued forest growth. Further, application of external compressive force to a growing forest can decrease the growth rate and cause significant defects in the CNTs themselves, yet the mechanical energy output of CNT growth in these experiments was orders of magnitude below the chemical energy of the C_2H_4 decomposition reaction.[51] A decrease in the self-supporting CNT−CNT interactions as the number density decays, as verified by the finite element model, may also permit growth of more defective CNT structures under stresses[52] present in the CNT forest, and this could accelerate the collective termination process.

Last, variation in the rate of density decay may underlie nonrepeatability of CNT forest height under identical growth times and conditions, which is widely discussed in this field but currently met with a lack of practical understanding. We find that the forest mass per unit area of substrate is far more repeatable in our process than the terminal forest height, suggesting that duration of the steady growth stage is far more repeatable than the duration of the density decay stage.

In conclusion, we propose a collective mechanism for the evolution and termination of CNT forest growth, which is supported experimentally by measurements of the time evolution of forest mass and height and mapping of the Hermans orientation parameter using synchrotron X-ray scattering. We present that forest growth consists of four stages: self-organization; steady growth with a constant CNT number density; decay with a decreasing number density; and abrupt termination, which is coincident with a loss of alignment at the base of the forest. Thus, termination is driven by a declining population density of CNTs, which deactivate individually yet must vitally support one another for collective growth to continue. The observed density decay would also considerably degrade the through-thickness properties of CNT forests, such as their electrical and thermal conductivity, and therefore, it is essential to consider the uniformity of forest density for future developments of these new materials. Our findings support previously unexplained observations of abrupt self-termination of SWNT and MWNT forest growth and may be generalized to further understand the collective growth mechanics of filamentary nanostructures. Thus, *in situ* monitoring of the CNT morphology and density during growth has the potential of providing a means for spotting the early indicators of a decay in the number density of growing CNTs. This information may be used to change the process parameters such as temperature, pressure, and the reaction environment to delay and/or eliminate growth termination.

Acknowledgment. .

This research was supported by the National Science Foundation (CMMI-0800213) and the University of Michigan Department of Mechanical Engineering and College of Engineering. E.R.M. is grateful for the support a University of Michigan Mechanical Engineering Departmental Fellowship. X-ray scattering was performed at the Cornell High-Energy Synchrotron Source (CHESS), which is supported by the National Science Foundation and the National Institutes of Health under Grant No. DMR-0225180. We thank Sameh Tawfick, Michael De Volder, Jong G. Ok, Sangwoo Han, Myounggu Park, Arthur Woll, Mark Tate, Hugh Philipp, Marianne Hromalik, and Sol Gruner for assistance with X-ray scattering experiments and analysis; and Yongyi Zhang for insightful discussions and support with CNT growth experiments.

Supporting Information Available: Detailed CNT growth methods of both the "hot wall" reactor and the "cold wall" reactor, Raman spectroscopy analysis of CNTs grown for 5 and 30 min in the "hot wall" reactor, and spatial mapping of CNT diameter across the height of a sample that was grown for 20 min in the "hot wall" reactor; further description of the finite element models of CNT−CNT buckling and contact. This material is available free of charge via the Internet at http://pubs.acs.org.

References and Notes

(1) Baughman, R. H.; Zakhidov, A. A.; de Heer, W. A. *Science* **2002**, *297*, 787.

(2) Puretzky, A. A.; Geohegan, D. B.; Jesse, S.; Ivanov, I. N.; Eres, G. *Appl. Phys. A* **2005**, *81*, 223.

(3) Lacava, A. I.; Bernardo, C. A.; Trimm, D. L. *Carbon* **1982**, *20*, 219.

(4) Stadermann, M.; Sherlock, S. P.; In, J.-B.; Fornasiero, F.; Park, H. G.; Artyukhin, A. B.; Wang, Y.; De Yoreo, J. J.; Grigoropoulos, C. P.; Bakajin, O.; Chernov, A. A.; Noy, A. *Nano Lett.* **2009**, *9*, 738.

(5) Zheng, L. X.; O'Connell, M. J.; Doorn, S. K.; Liao, X. Z.; Zhao, Y. H.; Akhadov, E. A.; Hoffbauer, M. A.; Roop, B. J.; Jia, Q. X.; Dye, R. C.; Peterson, D. E.; Huang, S. M.; Liu, J.; Zhu, Y. T. *Nat. Mater.* **2004**, *3*, 673.

(6) Dresselhaus, M. S.; Dresselhaus, G.; Avouris, P. *Carbon nanotubes: synthesis, structure, properties, and applications*; Springer: Berlin; New York, 2001.

(7) Garcia, E. J.; Wardle, B. L.; Hart, A. J. *Composites Part A: Appl. Sci. Manufactur.* **2008**, *39*, 1065.

(8) Tong, T.; Zhao, Y.; Delzeit, L.; Kashani, A.; Meyyappan, M.; Majumdar, A. *IEEE Trans. Compon. Packag. Technol.* **2007**, *30*, 92.

(9) Pushparaj, V. L.; Ci, L. J.; Sreekala, S.; Kumar, A.; Kesapragada, S.; Gall, D.; Nalamasu, O.; Pulickel, A. M.; Suhr, J. *Appl. Phys. Lett.* 2007, *91*.

(10) Pushparaj, V. L.; Shaijumon, M. M.; Kumar, A.; Murugesan, S.; Ci, L.; Vajtai, R.; Linhardt, R. J.; Nalamasu, O.; Ajayan, P. M. *Proc. Natl. Acad. Sci. U.S.A.* **2007**, *104*, 13574.

(11) Fornasiero, F.; Park, H. G.; Holt, J. K.; Stadermann, M.; Grigoropoulos, C. P.; Noy, A.; Bakajin, O. *Proc. Natl. Acad. Sci. U.S.A.* **2008**, *105*, 17250.

(12) Holt, J. K.; Park, H. G.; Wang, Y. M.; Stadermann, M.; Artyukhin, A. B.; Grigoropoulos, C. P.; Noy, A.; Bakajin, O. *Science* **2006**, *312*, 1034.

(13) Majumder, M.; Chopra, N.; Andrews, R.; Hinds, B. J. *Nature* **2005**, *438*, 44.

(14) Nednoor, P.; Gavalas, V. G.; Chopra, N.; Hinds, B. J.; Bachas, L. G. *J. Mater. Chem.* **2007**, *17*, 1755.

(15) Zhang, G. Y.; Mann, D.; Zhang, L.; Javey, A.; Li, Y. M.; Yenilmez, E.; Wang, Q.; McVittie, J. P.; Nishi, Y.; Gibbons, J.; Dai, H. J. *Proc. Natl. Acad. Sci. U.S.A.* **2005**, *102*, 16141.

(16) Hata, K.; Futaba, D. N.; Mizuno, K.; Namai, T.; Yumura, M.; Iijima, S. *Science* **2004**, *306*, 1362.

(17) Magrez, A.; Seo, J. W.; Kuznetsov, V. L.; Forro, L. *Angew. Chem., Int. Ed.* **2007**, *46*, 441.

(18) Nasibulin, A. G.; Brown, D. P.; Queipo, P.; Gonzalez, D.; Jiang, H.; Kauppinen, E. I. *Chem. Phys. Lett.* **2006**, *417*, 179.

(19) Wei-Hung Chiang, R.M. S. *Adv. Mater.* **2008**, *20*, 4857.

(20) Wang, S. W.; Borisevich, A. Y.; Rashkeev, S. N.; Glazoff, M. V.; Sohlberg, K.; Pennycook, S. J.; Pantelides, S. T. *Nat. Mater.* **2004**, *3*, 143.

(21) Shanov, V. N.; Gorton, A.; Yun, Y.-H.; Schultz, M. J. Composite Catalyst and Method for Manufacturing Carbon Nanostructured Materials, US Patent Application 2008/095695.

(22) Meshot, E. R.; Hart, A. J. *Appl. Phys. Lett.* 2008, *92*.

(23) Shanov, V.; Mallik, N.; Chu, W.; Li, W.; Jayasinghe, C.; Yun, Y.; Schulz, M. J.; Yarmolenko, S.; Salunke, P.; Li, G. *Advances in Synthesis and Application of Carbon Nanotube Materials Materials Science and Technology Conference*, Pittsburgh, PA, 2008.

(24) Puretzky, A. A.; Eres, G.; Rouleau, C. M.; Ivanov, I. N.; Geohegan, D. B. *Nanotechnology* 2008, *19*.

(25) Mattevi, C.; Wirth, C. T.; Hofmann, S.; Blume, R.; Cantoro, M.; Ducati, C.; Cepek, C.; Knop-Gericke, A.; Milne, S.; Castellarin-Cudia, C.; Dolafi, S.; Goldoni, A.; Schloegl, R.; Robertson, J. *J. Phys. Chem. C* **2008**, *112*, 12207.

(26) Patole, S. P.; Alegaonkar, P. S.; Lee, H. C.; Yoo, J. B. *Carbon* **2008**, *46*, 1987.

(27) Wu, J.; Huang, Q. W.; Ma, Y. F.; Huang, Y.; Liu, Z. F.; Yang, X. Y.; Chen, Y. S.; Chen, D. P. *Colloids Surf., A* **2008**, *313*, 13.

(28) Hart, A. J.; van Laake, L.; Slocum, A. H. *Small* **2007**, *3*, 772.

(29) van Laake, L.; Hart, A. J.; Slocum, A. H. *Rev. Sci. Instrum.* 2007, *78*.

(30) Zhang, L.; Li, Z. R.; Tan, Y. Q.; Lolli, G.; Sakulchaicharoen, N.; Requejo, F. G.; Mun, B. S.; Resasco, D. E. *Chem. Mater.* **2006**, *18*, 5624.

(31) Su, C. J.; Hwang, D. W.; Lin, S. H.; Jin, B. Y.; Hwang, L. P. *Physchemcomm* **2002**, *5*, 34.

(32) Wang, B. N.; Bennett, R. D.; Verploegen, E.; Hart, A. J.; Cohen, R. E. *J. Phys. Chem. C* **2007**, *111*, 17933.

(33) Wang, B. N.; Bennett, R. D.; Verploegen, E.; Hart, A. J.; Cohen, R. E. *J. Phys. Chem. C* **2007**, *111*, 5859.

(34) Zhu, L. B.; Hess, D. W.; Wong, C. P. *J. Phys. Chem. B* **2006**, *110*, 5445.

(35) Zhu, L. B.; Xu, J. W.; Xiao, F.; Jiang, H. J.; Hess, D. W.; Wong, C. P. *Carbon* **2007**, *45*, 344.

(36) Patole, S. P.; Park, J. H.; Lee, T. Y.; Lee, J. H.; Patole, A. S.; Yoo, J. B. *Appl. Phys. Lett.* 2008, *93*.

(37) Yasuda, S.; Hiraoka, T.; Futaba, D. N.; Yamada, T.; Yumura, M.; Hata, K. *Nano Lett.* **2009**, *9*, 769.

(38) Meshot, E. R.; Plata, D. L.; Tawfick, S.; Zhang, Y. Y.; Verploegen, E. A.; Hart, A. J. *Acs Nano* **2009**, *3*, 2477.

(39) Bedewy, M.; Meshot, E. R.; Lyons, K.; Woll, A. R.; Juggernauth, K. A.; Tawfick, S.; Hart, A. J. Submitted 2009.

(40) Eres, G.; Kinkhabwala, A. A.; Cui, H. T.; Geohegan, D. B.; Puretzky, A. A.; Lowndes, D. H. *J. Phys. Chem. B* **2005**, *109*, 16684.

(41) Amama, P. B.; Pint, C. L.; McJilton, L.; Kim, S. M.; Stach, E. A.; Murray, P. T.; Hauge, R. H.; Maruyama, B. *Nano Lett.* **2009**, *9*, 44.

(42) Nishino, H.; Yasuda, S.; Namai, T.; Futaba, D. N.; Yamada, T.; Yumura, M.; Iijima, S.; Hata, K. *J. Phys. Chem. C* **2007**, *111*, 17961.

(43) Futaba, D. N.; Hata, K.; Yamada, T.; Mizuno, K.; Yumura, M.; Iijima, S. *Phys. Rev. Lett.* 2005, *95*.

(44) Pint, C. L.; Pheasant, S. T.; Parra-Vasquez, A. N. G.; Horton, C.; Xu, Y. Q.; Hauge, R. H. *J. Phys. Chem. C* **2009**, *113*, 4125.

(45) Yamada, T.; Maigne, A.; Yudasaka, M.; Mizuno, K.; Futaba, D. N.; Yumura, M.; Iijima, S.; Hata, K. *Nano Lett.* **2008**, *8*, 4288.

(46) Futaba, D. N.; Hata, K.; Namai, T.; Yamada, T.; Mizuno, K.; Hayamizu, Y.; Yumura, M.; Iijima, S. *J. Phys. Chem. B* **2006**, *110*, 8035.

(47) Zhang, Y.; Gregoire, J.; Hart, A. J. In preparation 2009.

(48) Zywitzki, O.; Hoetzsch, G. *Surf. Coat. Technol.* **1997**, *94*−*95*, 303.

(49) Noda, S.; Hasegawa, K.; Sugime, H.; Kakehi, K.; Zhang, Z. Y.; Maruyama, S.; Yamaguchi, Y. *Jpn. J. Appl. Phys., Part 2* **2007**, *46*, L399.

(50) Han, J. H.; Graff, R. A.; Welch, B.; Marsh, C. P.; Franks, R.; Strano, M. S. *Acs Nano* **2008**, *2*, 53.

(51) Hart, A. J.; Slocum, A. H. *Nano Lett.* **2006**, *6*, 1254.

(52) Zhang, Q.; Zhou, W. P.; Qian, W. Z.; Xiang, R.; Huang, J. Q.; Wang, D. Z.; Wei, F. *J. Phys. Chem. C* **2007**, *111*, 14638.

JP904152V

SUPPORTING INFORMATION for

Collective mechanism for the evolution and self-termination of vertically aligned carbon nanotube growth

Mostafa Bedewy[1], *Eric R. Meshot*[1], *Haicheng Guo*[1], *Eric A. Verploegen*[2], *Wei Lu*[1], *A. John Hart*[1*]

[1]Department of Mechanical Engineering, University of Michigan, 2350 Hayward Street, Ann Arbor, MI 48109 USA.

[2]Department of Materials Science and Engineering, Massachusetts Institute of Technology, 77 Massachusetts Avenue, Cambridge, MA 02139 USA.

*ajohnh@umich.edu

RECEIVED DATE (to be automatically inserted after your manuscript is accepted if required according to the journal that you are submitting your paper to)

CORRESPONDING AUTHOR: A. John Hart, ajohnh@umich.edu, 734.615.6146 (O), 734.764.5751 (F).

CNT growth methods

Figures S1 and S2 show the time-temperature-flow sequences for CNT forest growth in our CVD systems. Source gases of He (99.999%, PurityPlus), H_2 (99.999%, PurityPlus), and C_2H_4 (99.999%, PurityPlus) were used.

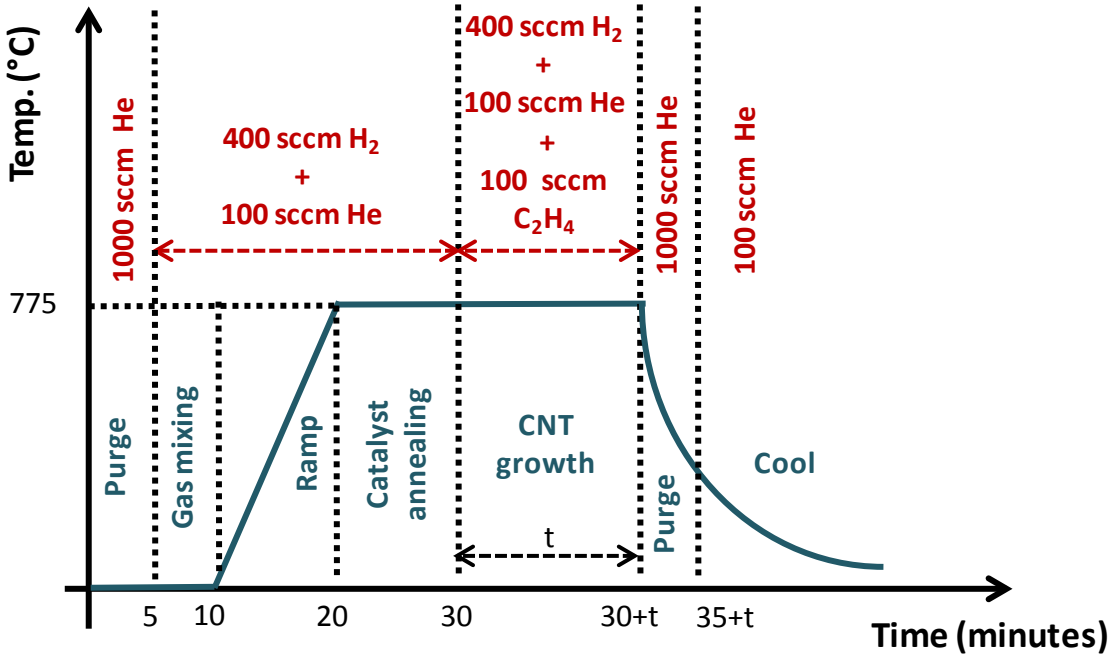

Figure S1. Process sequence for growth of CNTs forests in a hot wall reactor (tube furnace) for growth time (*t*) varying from 2.5 to 30 minute s.

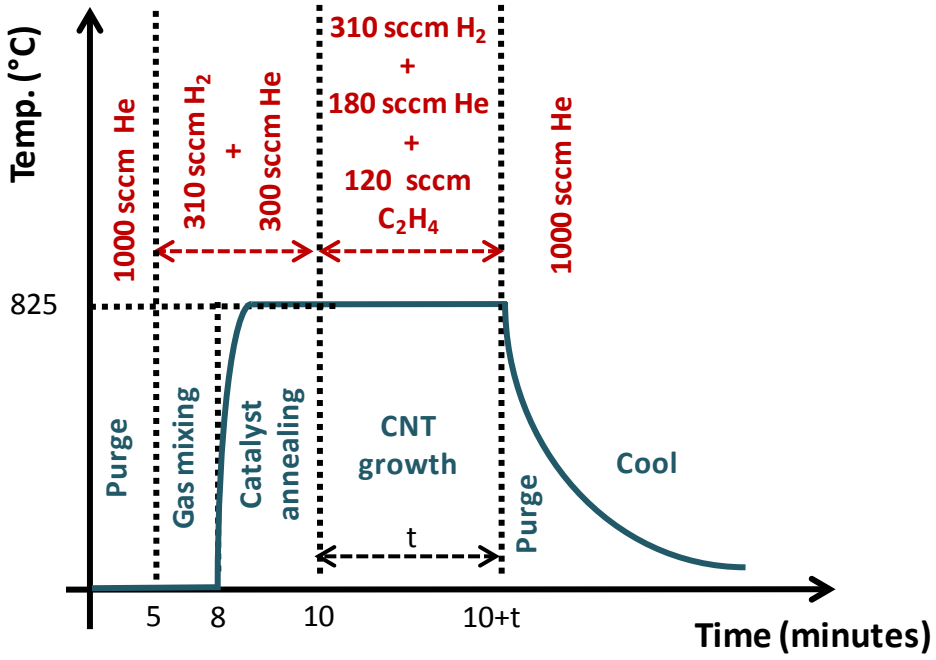

Figure S2. Process sequence for growth of CNTs forests in a cold wall reactor, which was mounted in the synchrotron beamline for X-ray scattering studies. During growth, the heated substrate is operated at T_s, while the thermal decomposition of the incoming gas mixture is determined by preheating upstream of the reactor at temperature T_p. First, a five-minute purging step is carried out to purge out air from the tube as a preparation step for introducing H_2; during this step, the preheater is ramped to the setpoint T_p= 1040°C. Then, a three-minute gas-mixing step is carried out to stabilize the gas atmosphere before heating. After that, the temperature is rapidly increased to T_s = 825°C in a period of approximately ten seconds.

Spatially-resolved measurement of CNT diameter

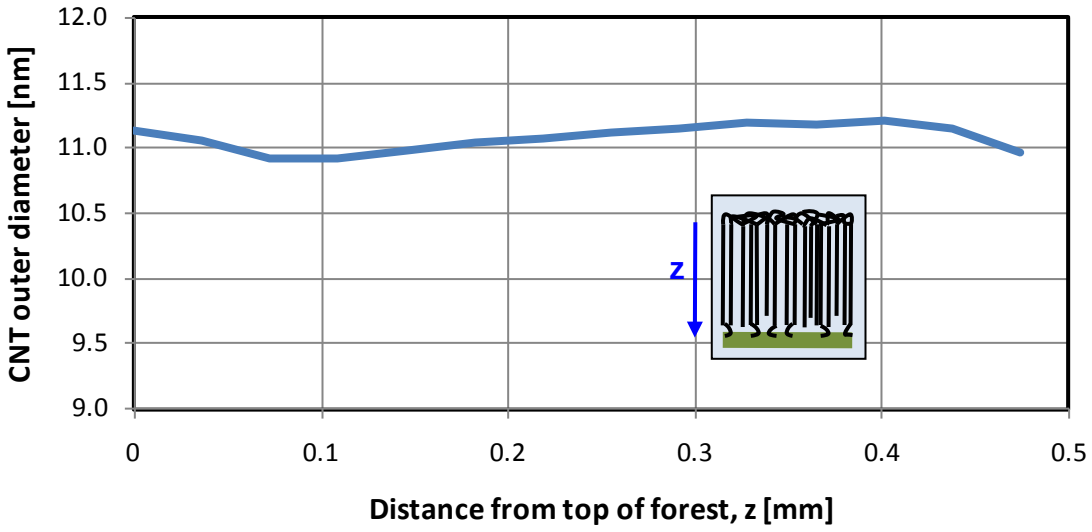

Figure S3. Spatially-resolved diameter map within a CNT forest that was grown for 20 minutes in the "hot wall" reactor. This data was obtained by fitting the SAXS patterns with a form factor model for a lognormally distributed population of hollow cylinders. The results show that the variation in diameter within a forest is less than 10%. The SAXS fitting algorithm assumes that the ratio of CNT inner to outer diameter is 0.6.

Analysis of CNT quality by Raman spectroscopy

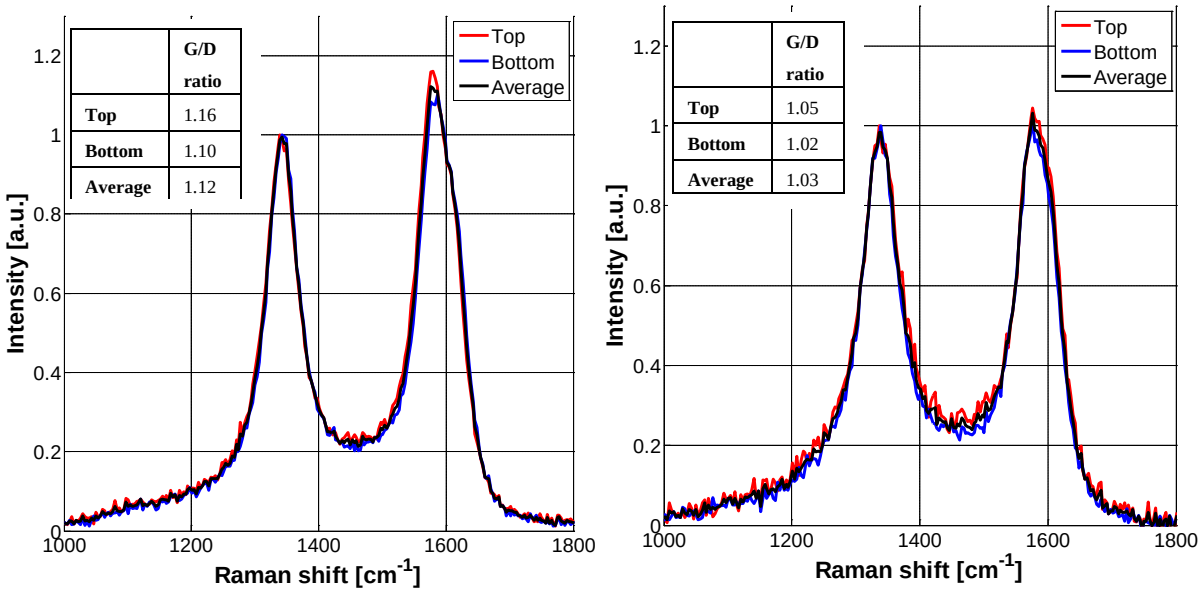

Figure S4. Raman spectra of CNT forests grown in the "hot wall" reactor for, (a) 5 minutes and (b) 30 minutes. The G/D ratio decreases slightly from the top to bottom of each sample, suggesting a slight decrease in CNT quality during the collective density decay. Also, the average quality of the CNT forest grown for 30 minutes, which is beyond self-termination, shows how apparent quality is not significantly reduced during the process.

Finite element model

Considering a model as shown in Figure S3, two CNTs are fixed to a rigid panel on the top and pinned to the substrate at the bottom. The rigid panel is subjected to a downward force. The length of the panel has dimensions $L = 500\text{nm}$, w = 80 nm and $t = 8\text{nm}$. The height of the CNTs is $h = 500$ nm. The CNTs are modeled as hollow cylinders with external diameter 10 nm and internal diameter 6 nm. The Young's modulus of the CNTs is 1 TPa, and Poisson ration is 0.3. The density of the cylinders is 2.2 g/cm^2 . The total force on the rigid panel is 2F = 1.6×10^{-7} N. In order to capture the trend of the displacement of the CNT forest with the increase of the number of CNTs, we change the distance *d* between two nanotubes from 500nm to 40nm, which corresponds to CNT density from 4×10^{8} to 5×10^{10} cm^{-2}. The commercial finite element package ABAQUS is employed and an 8-node linear solid element C3D8R with reduced integration is used to model the CNTs.

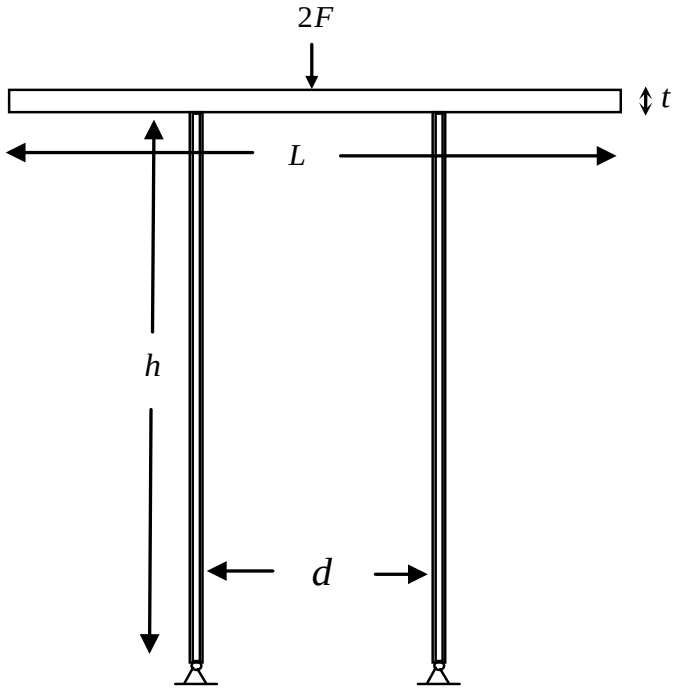

Figure S5. Illustration of a two-CNT model under compression

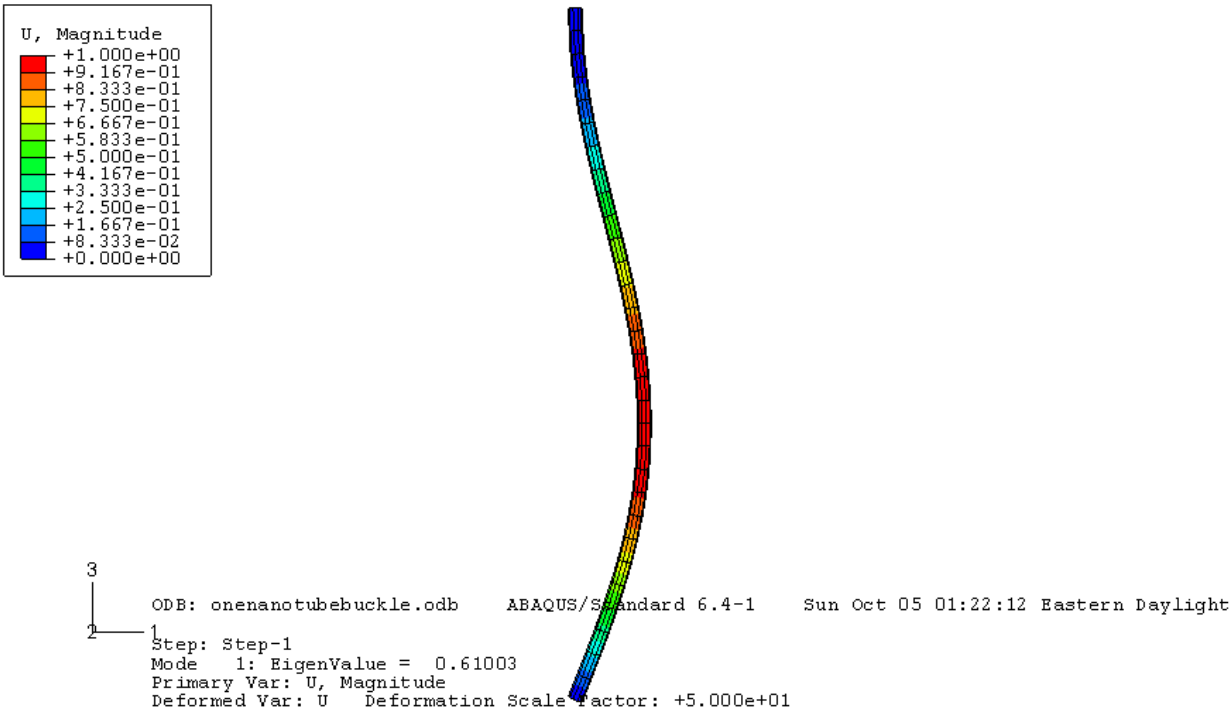

Figure S6. The first buckling mode of an individual CNT under compression. The CNT is pinned at the bottom and fixed to a rigid top panel as shown in Fig. S3.

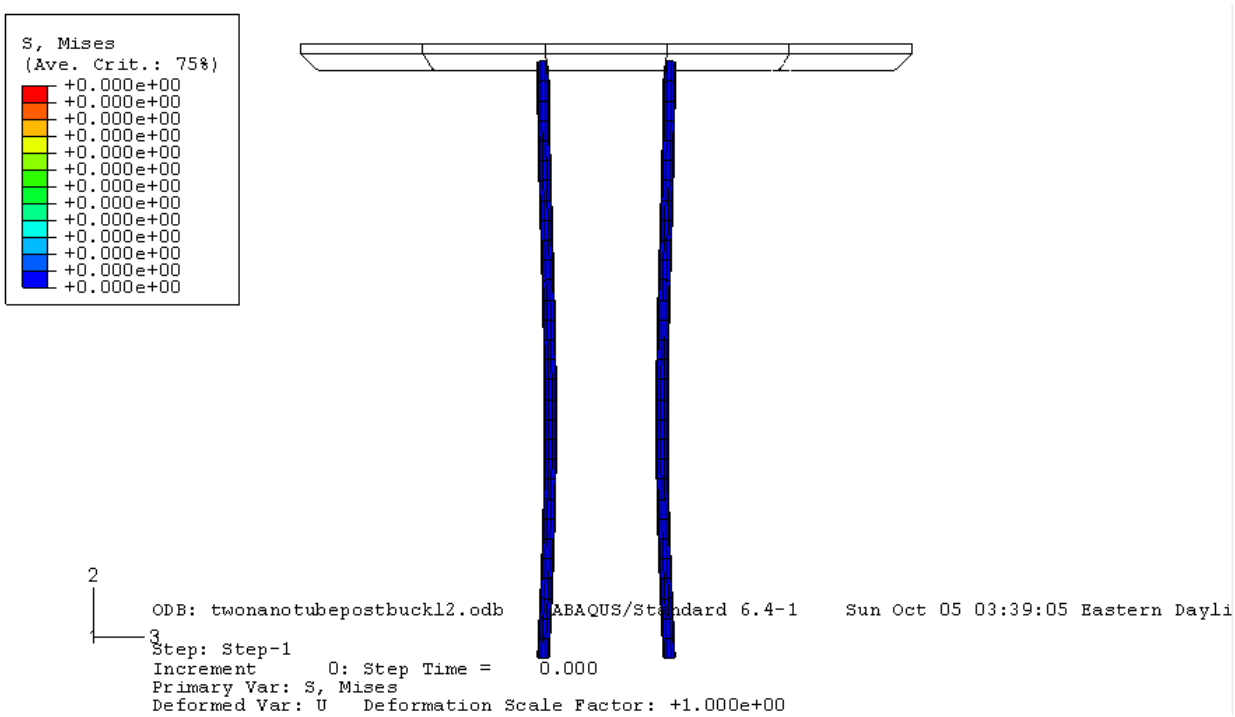

Figure S7. The model used in post-buckling analysis, where the buckled shape was used as a starting imperfection for the pair of CNTs.

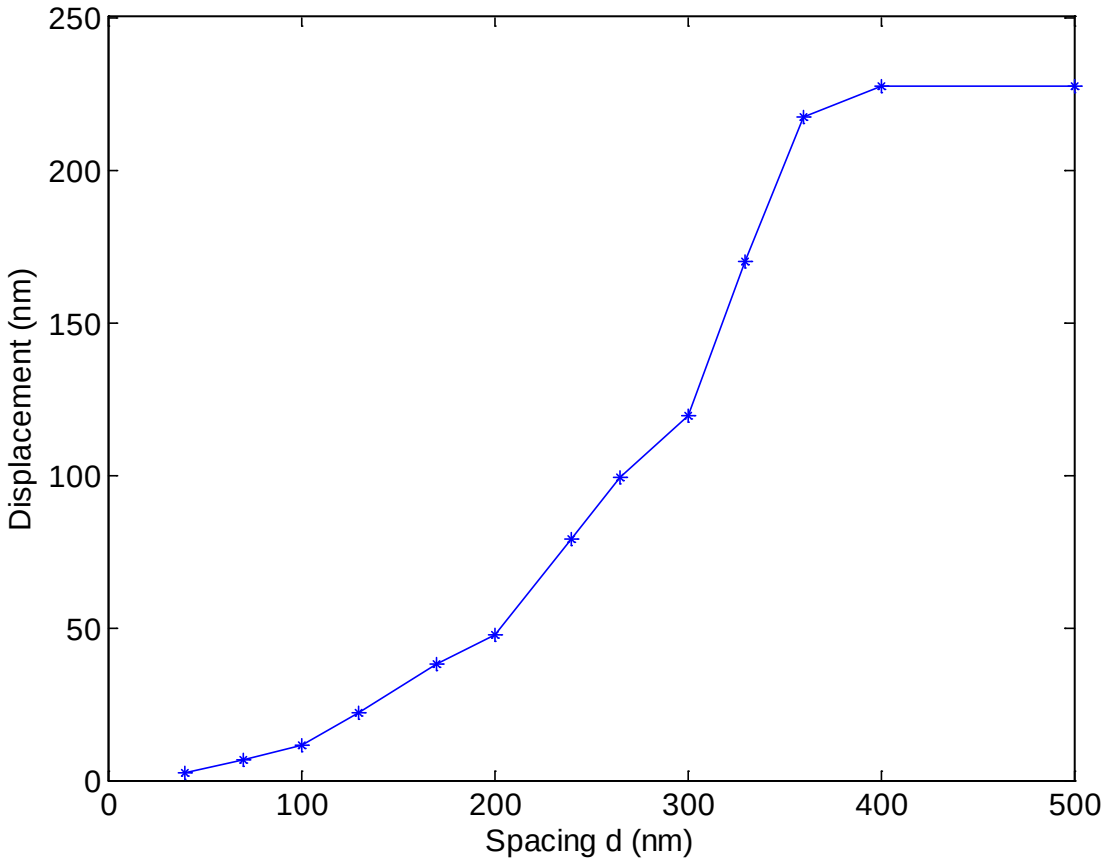

Figure S8. Plot of panel displacement as a function of the spacing *d* between a pair of CNTs. When *d* is larger than 400 nm, the CNTs do not contact each other during the whole post-buckling deformation process, and the overall displacement of the system remains the same. When the spacing *d* decreases from 360 to 40 nm, the nanotubes contact each other and the self-supporting structure is maintained with good alignment. The sharp decrease in panel displacement for *d* less than 360 n marks the sudden transition between the aligned and unaligned morphologies.

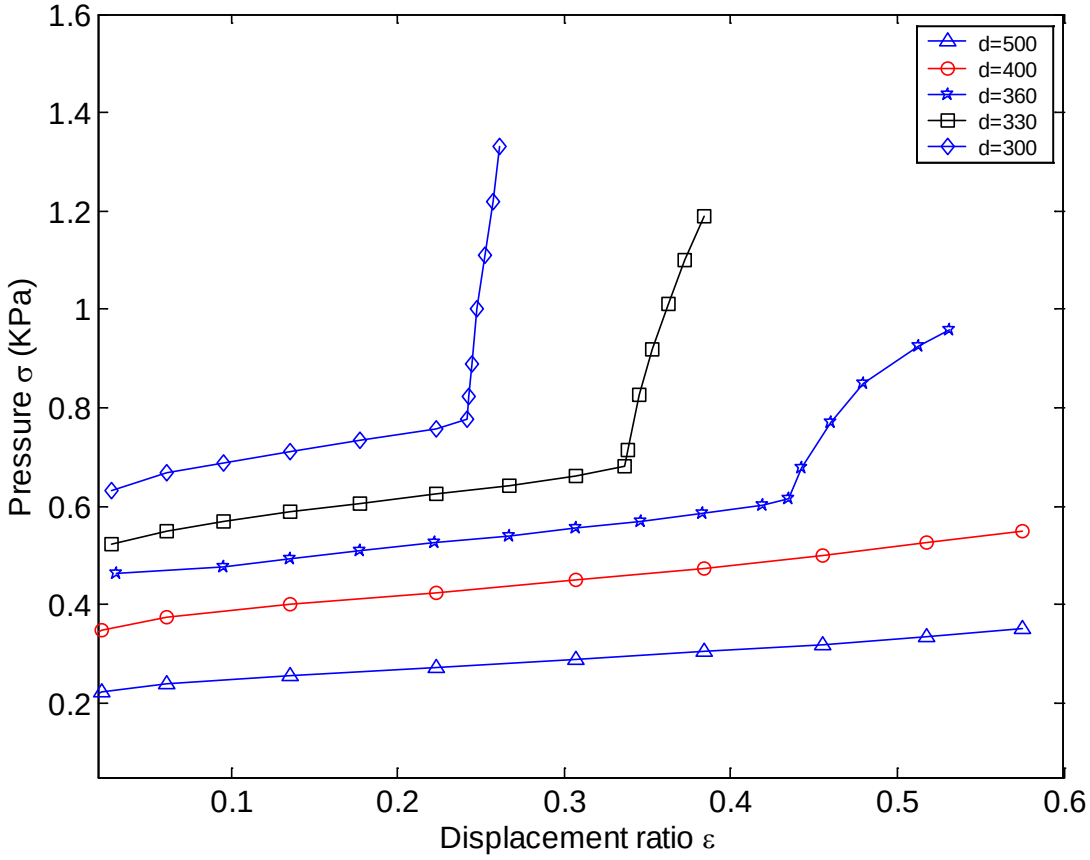

Figure S9. Plot of pressure (σ) applied to the top panel vs. the ratio (ε) of relative displacement. The sharp increase in the slope of the σ–ε relationship for cases where $d \leq 360$ nm indicates stiffening due to CNT-CNT contact.